communications biology

A Nature Portfolio journal

Article

https://doi.org/10.1038/s42003-025-08261-y

Human placenta mesenchymal stromal cells alleviate intestinal inflammation and repair intestinal barrier function by activating AMPK-FXR pathway

Ruo Wang[1,6], Bing Feng[1,6], Qigu Yao[1], Qiaoling Pan[1], Jiong Yu[1,2,3], Chaoxu Liu[4], Jinhai Wang[4], Lanjuan Li[1,2], Hongcui Cao[1,5] ✉ & Jue Xie[1,3,5] ✉

Crohn's disease (CD) has a complex pathogenesis; there is currently no effective treatment. Mesenchymal stromal cells (MSCs) are a potential therapeutic option for CD. It is important to systematically evaluate the safety and effectiveness of MSCs and their mechanism for the treatment of CD to support their clinical application. Here, the safety and effectiveness of MSCs from the human placenta (hPMSCs) are evaluated. All the indicators show that hPMSC transplantation is safe and effectively alleviates intestinal inflammation, reduces intestinal apoptosis and fibrosis, and promotes recovery of the intestinal barrier in mice and organoids. IGFBP-4 is the most expressed by hPMSCs and is verified to play a therapeutic role by activating the AMPK-FXR pathway to alleviate intestinal inflammation and repair the intestinal barrier function. Our findings demonstrate that hPMSCs alleviate CD by activating the AMPK-FXR pathway with IGFBP-4 to reduce intestinal inflammation and repair intestinal barrier function.

Crohn's disease (CD), a type of inflammatory bowel disease (IBD), is characterized by chronic and relapsing inflammation in the gastrointestinal tract[1]. Patients with CD suffer from abdominal pain, fever, diarrhea, and weight loss[2]. Most patients are diagnosed when they are young and have substantial healthcare costs with a low quality of life[3]. The understanding of CD pathogenesis is still poor. A complex interaction involving genetic, environmental, and microbial factors and the immune response is thought to cause this disease[4]. Currently, treatments for CD focus on inducing and maintaining remission of patient inflammation, instead of targeting the pathogenic mechanism. In addition, side effects of these drugs should not be ignored including adrenal insufficiency, intercurrent infection, inhibition of cell proliferation, and liver injury[5,6]. Finally, the significant cost and high relapse rate are important considerations for some patients[7]. Therefore, stem/stromal cell therapy may be a viable option for CD.

Mesenchymal stromal cells (MSCs) are non-hematopoietic multipotent stromal cells that can self-renew and differentiate into a variety of mesodermal tissues, such as adipocytes, chondrocytes, and osteoblasts[8–11]. They regulate inflammation and promote repair by secreting different cytokines or extracellular vesicles (EVs)[12–14], indicating that their use may be a good way to suppress inflammation and repair wounded tissue in CD. More than 700 clinical trials have identified the immunosuppressive ability of MSCs in different kinds of autoimmune diseases, such as graft-versus-host disease (GVHD), multiple sclerosis, and systemic lupus[15], etc. Many CD clinical trials have also been performed[16,17]. However, given the limited understanding of the mechanisms underlying MSC-based therapy for CD and the absence of comprehensive preclinical studies to establish optimal treatment protocols, a subset of patients exhibited either no therapeutic response to MSC treatment or experienced disease progression necessitating surgical intervention

[1]State Key Laboratory for the Diagnosis and Treatment of Infectious Diseases, National Clinical Research Center for Infectious Diseases, National Medical Center for Infectious Diseases, Collaborative Innovation Center for Diagnosis and Treatment of Infectious Diseases, The First Affiliated Hospital, Zhejiang University School of Medicine, 79 Qingchun Rd, Hangzhou City, China. [2]Jinan Microecological Biomedicine Shandong Laboratory, Jinan City, China. [3]Department of Blood Transfusion, The First Affiliated Hospital, Zhejiang University School of Medicine, 79 Qingchun Rd, Hangzhou City, China. [4]Department of Colorectal Surgery, The First Affiliated Hospital, Zhejiang University School of Medicine, 79 Qingchun Rd, Hangzhou City, China. [5]Zhejiang Key Laboratory for Diagnosis and Treatment of Physic-chemical and Aging-related Injuries, 79 Qingchun Rd, Hangzhou City, China. [6]These authors contributed equally: Ruo Wang, Bing Feng.
✉e-mail: hccao@zju.edu.cn; zyyyxj2011@zju.edu.cn

following therapy. To determine the optimal scheme and a novel mechanism for MSCs in the treatment of CD, systematic preclinical evaluation, including safety and effectiveness, and in-depth study on the mechanism are needed to follow-up clinical trials evaluating MSC treatment.

Extensive studies have demonstrated that insulin-like growth factor-binding proteins (IGFBPs) play a crucial role in promoting intestinal epithelial cell (IEC) regeneration and enhancing wound healing processes. These properties position IGFBPs as promising therapeutic candidates for IBD, offering dual benefits of mitigating intestinal inflammation and stimulating IEC proliferation[18]. IGFBPs inhibit IGF actions by preventing binding to IGF receptors in most circumstances, they also could modulate cell proliferation, survival, differentiation, migration, and invasion independent of IGFs[19–21]. IGFBP-4, as the smallest and unique member among the human IGFBPs, could inhibit the growth of prostate cancer cells, lung adenocarcinomas and giant cell tumor-derived stromal cells by an IGF-dependent pathway[22–24]. IGFBP-4 could also regulate cardiomyocyte differentiation and decrease ischemic injury after myocardial infarction in an IGF-independent way[25,26]. Yet the role of IGFBP-4 in CD remained unknown.

It has been documented that inflammation is regulated by a complex network of signaling pathways, such as AMP-activated protein kinase (AMPK) and NF-κB-mediated signaling. AMPK is a multi-substrate serine/threonine protein kinase that plays a regulatory role in oxidative stress, inflammation, autophagy, mitochondrial dysfunction, and cellular fate[27]. Farnesoid X-receptor (FXR), mainly expressed in the liver and intestine, is a bile acid-activated nuclear receptor, that regulates the genes for the metabolic process of bile acid synthesis, transport and reabsorption and could be modulated by AMPK[28,29]. Some research has documented that the expression of FXR in the intestines of IBD patients is reduced, resulting in bile acid metabolism disorders and serious intestinal inflammation[30,31]. Some studies have suggested that phosphorylation of AMPK can activate FXR in the liver and kidney[29], but the relationship between AMPK and FXR in the intestine has not been evaluated.

In this study, the SAMP1/Yit mouse, the animal model that best simulates the pathological process and features of human CD at present[32], a dextran sulfate sodium (DSS)-induced acute colitis mouse model, and intestinal organoids from CD patients and SAMP1/Yit mice were used to systematically evaluate the safety and efficacy of hPMSC transplantation to treat CD and find the mechanism for hPMSCs in the treatment of CD.

Results

Intraperitoneal hPMSCs were primarily recruited to the inflammatory site of the terminal ileum in SAMP1/Yit mice and proved to be safe

hPMSCs were identified by the potential ability of multi-directional differentiation and specific surface markers (Supplementary Fig. 1). The results of biological distribution, toxic reaction, abnormal immune response, and oncogenicity were used to evaluate the safety of hPMSCs based on the Standards of clinical-grade mesenchymal stromal cell preparation and quality control (2020 China Version)[33]. Fluorescence emitted by DiR-labeled hPMSCs was observed at various time points (days 1, 3, 5, 7, 14, and 21) post-injection. In SAMP1/Yit mice, the fluorescence signal was predominantly localized within the abdominal cavity. In contrast, in AKR/J mice, the positive signal was primarily detected at the injection site or within the spleen, with the intensity progressively diminishing from day 1 through day 21 following injection (Fig. 1A). Fluorescence intensity in SAMP1/Yit mice was quantified which showed that the intensity gradually weakened from day1 to 21 after injection, and the fluorescence signal was essentially nonexistent in vivo at day 21 after injection (Fig. 1B). The positive signal was primarily focused on the terminal ileum of SAMP1/Yit mice while only in the spleen of AKR/J mice (Fig. 1C). Large numbers of red fluorescence signals were observed in the lamina propria of the ileum (Fig. 1D).

Body temperature, food, and water consumption of AKR/J mice injected with hPMSCs were in the normal range after 1 week and 8 weeks of observation to evaluate acute and long-term toxic reactions. The ratios of organ weight to body weight were also normal (Supplementary Fig. 2A). There were also no abnormal changes in the body weight curve of mice after 8 weeks of observation (Supplementary Fig. 2B). No pathological changes in the livers, terminal ileums, or kidneys of the mice were observed (Supplementary Fig. 2C). Finally, blood biochemistry analysis showed that liver function, renal function, and lipid metabolism of each group were all within normal levels (Supplementary Fig. 2D and E).

The number of Treg cells and the percentage of $CD4^+/CD8^+$ T cells in mice injected with hPMSCs were not significantly different from those of non-transplanted mice (Supplementary Fig. 3A–B). The levels of tumor necrosis factor (TNF)-α, Interleukin (IL)-1β, and IL-6 were lower than or equal to those of mice without hPMSC injection (Supplementary Fig. 3C).

No tumors were observed in any of the organs of AKR/J mice and SCID mice injected with hPMSCs (Supplementary Fig. 4A and B). The body weight curve of SCID mice injected with hPMSCs increased during the first 4 weeks and then leveled off (Supplementary Fig. 4C).

Intraperitoneal hPMSC treatment proved to be therapeutic in two distinct CD mouse models

Two distinct CD mouse models (DSS-induced acute colitis mouse model and SAMP1/Yit mice) were used to evaluate the effectiveness of hPMSCs.

After 1 week of treatment, the pathological analysis indicated that inflammation of the terminal ileum was alleviated, as indicated by decreased muscularis propria and submucosal thickness, an increased intestinal villus height (Fig. 2A). A lighter inflammatory cell infiltration and less neutrophil recruitment were shown by the decreased positive areas of immunohistochemical staining of myeloperoxidase (MPO) and Ly6G. The expression of S100A8 and S100A9, as reliable biomarkers of inflammation, also decreased after hPMSC treatment (Fig. 2B). A reduced trend of the expression of the inflammatory factors TNF-α, IL-1β, and IL-6 was also shown after injecting hPMSCs for 1 week (Fig. 2C). FITC fluorescence intensity in the blood significantly decreased after cell transplantation, which meant that the intestinal barrier function was improved after the hPMSC treatment (Fig. 2D). Immunohistochemical analysis of tight junction proteins Claudin-1 (Cldn1) and Claudin-2 (Cldn2) also showed that hPMSC transplantation promoted recovery of the intestinal barrier in SAMP1/Yit mice. Terminal deoxynucleotidyl transferase dUTP Nick-End Labeling(TUNEL) staining and immunohistochemical analysis of alpha smooth muscle actin (α-SMA) showed that intestinal apoptosis and fibrosis were both alleviated following hPMSC transplantation (Fig. 2E).

SAMP1/Yit mice were injected with 2×10^6 of hPMSCs were observed for 8 weeks; the body weight of hPMSC-injected mice remained stable, while that of mice not injected with hPMSCs decreased with age (Supplementary Fig. 5A). Pathological analysis of the terminal ileum showed significant improvement in submucosal and muscle layer thickness, and the degree of inflammatory cell infiltration in hPMSC-injected mice (Supplementary Fig. 5B). Additionally, immunohistochemical analysis of α-SMA demonstrated a marked reduction in intestinal fibrosis 8 weeks after hPMSC transplantation (Supplementary Fig. 5C).

The therapeutic effect of hPMSCs was also evaluated in the DSS-induced acute colitis mouse model (Fig. 3A). Compared with mice in the DSS group, DSS mice injected with hPMSCs had less weight loss and longer colons (Fig. 3B–D). TUNEL staining showed that the number of apoptotic cells decreased after treatment (Fig. 3E and F). Pathological and MPO immunohistochemical analyses showed that the number of infiltrated inflammatory cells significantly decreased and the pathological score of mice injected with hPMSCs decreased (Fig. 3E, G and H). Following hPMSC transplantation, gene and protein expression of the tight junction protein Cldn1 increased but Cldn2 decreased, indicating hPMSC transplantation promoted recovery of the intestinal barrier (Fig. 3I and J). Extraction of colon RNA revealed that expression of inflammatory factors also decreased after treatment (Supplementary Fig. 6).

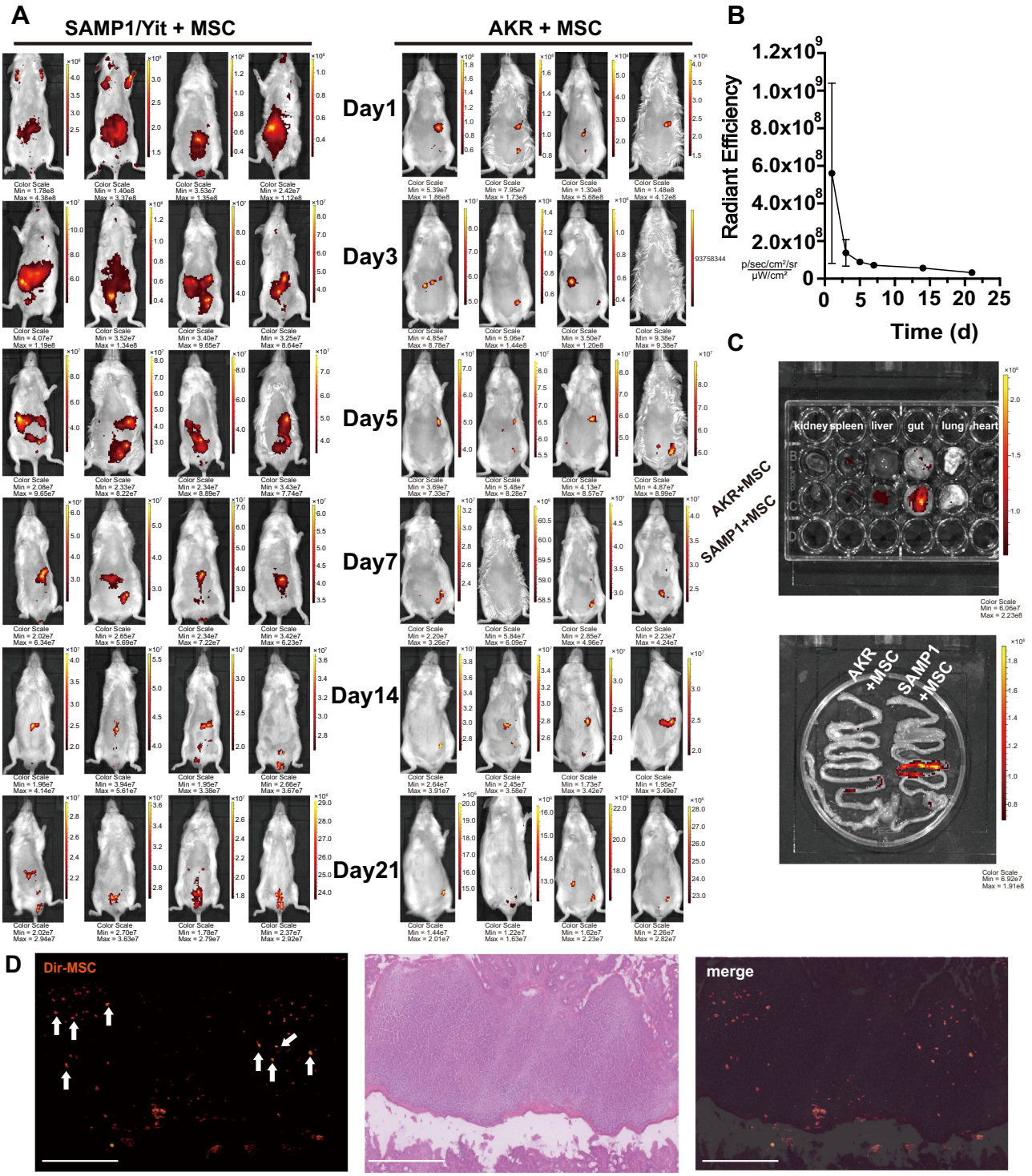

Fig. 1 | Aggregation of hPMSCs at the inflammatory site of ileitis in mice. A In vivo tracing of hPMSCs on days 1, 3, 5, 7, 14, and 21 after hPMSC injection. Labeled hPMSCs were detected with an IVIS imaging system. Brighter colors indicate increased cell accumulation. ($n = 4$ in each group). **B** Quantification of DiR fluorescent radiance in the whole body over time. **C** Images of DiR fluorescent radiance in different organs and concentrated on the inflamed portion of the whole gut. **D** Large numbers of hPMSCs migrated in the muscularis of the inflamed part of the whole gut (merge of histological and fluorescence images). Arrow: hPMSCs (10×, scale bar, 250 μm). Data were presented as mean ± standard deviation (SD).

hPMSCs promoted proliferation, inhibited apoptosis, and recovered barrier function in both Orgs^{CD} and Orgs^{SAMP1}

Crypts from CD patients were isolated and organoids (named as Orgs^{CD}) were successfully cultured (Fig. 4A, B). Mature intestinal organoids could be formed on the seventh day of culture (Fig. 4B). Cultured intestinal organoids contain colonocytes (CK20), goblet cells (MUC2), Paneth cells (lysozyme), and enteroendocrine cells (Chromogranin A), demonstrating that the organoids we cultured were mature (Fig.4C). Epithelial turnover was present in organoids and characterized by proliferating cell nuclear antigen (PCNA) staining in proliferative zones and caspase-3 staining in apoptotic zones (Fig. 4C). The size of Orgs^{CD} was smaller than intestinal organoids derived from health control (named as Orgs^{Health}) (Fig. 4D).

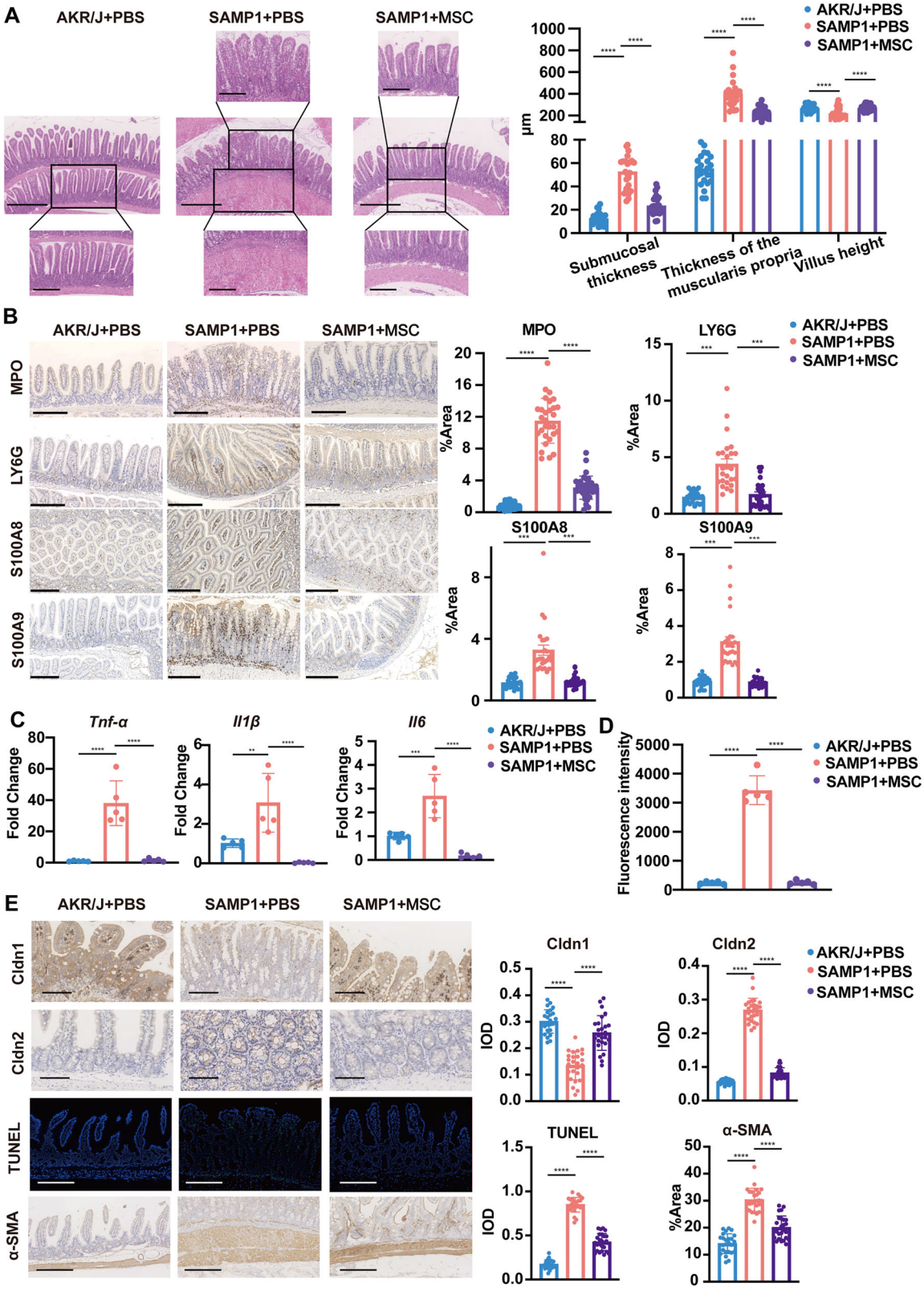

In order to discover the epithelial permeability of Orgs^{CD}, FD4 was added in culture medium of Orgs^{CD}. The intensity of green fluorescence in the Orgs^{CD} lumen is not obviously different compared with Orgs^{Health}. The gene levels of tight junction protein CLDN1 and CLDN2 were also the same as Orgs^{Health}, which indicated that Orgs^{CD} lost their inflammatory status and needed cytokines to recreate a more physiological microenvironment (Supplementary Fig. 7).

An in vitro co-culture system was established for further experiments, with hPMSCs in the lower layer and organoids cultured in the transwells (Fig. 4E). TNF-α, which has been implicated as a critical contributor in

Fig. 2 | Therapeutic effects of hPMSC transplantation in mice. A Representative hematoxylin-eosin (H&E) images (5×) of terminal ileum sections of AKR/J mice and SAMP1/Yit mice treated with PBS, 2×10^6 hPMSCs were shown (Scale bar, 500 μm). Zoomed images are at 10× magnification (Scale bar, 250 μm). Muscularis propria, submucosal thickness, and villus height of AKR/J mice, PBS and 2×10^6 hPMSCs-treated SAMP1/Yit mice were measured in five random views per mouse for quantitative analysis. **B** Representative immunohistochemical images for MPO, Ly6G, S100A8, and S100A9 (10×, scale bar, 250 μm) in each group. The positive areas of MPO, Ly6G, S100A8, and S100A9 expression were measured in five random views per mouse for quantitative analysis. **C** Gene expression levels of TNF-α, IL-1β, and IL-6 in each group (five mice in each group). **D** Fluorescence intensity of FITC in serum of each group (five mice in each group). **E** Representative immunohistochemical images and quantitative analysis for Cldn1 (20×, scale bar, 100 μm), Cldn2 (20×, scale bar, 100 μm), TUNEL (10×, scale bar, 250 μm) and α-SMA (10×, scale bar, 250 μm) in each group. Five fields were randomly selected from five mice for quantitative analysis. Results were presented as mean ± SD. $^*P < 0.05$, $^{**}P < 0.01$, $^{***}P < 0.001$, $^{****}P < 0.0001$; n.s., not significant. Five mice per group were used. After hPMSC transplantation, intestinal inflammation of mice was alleviated, inflammatory cell infiltration was reduced, the number of apoptotic cells was reduced, fibrosis was decreased, and the intestinal barrier was restored.

perpetuating intestinal inflammation in CD, was added to culture system while co-culturing with hPMSCs to stimulate $Orgs^{CD}$. The size of $Orgs^{CD}$ treated with TNF-α in advance continuously rose with increasing co-culture time with hPMSCs (Fig. 4F).

When FD4 was added to the system, the intensity of green fluorescence in the lumen of $Orgs^{CD}$ treated with TNF-α was increased, showing that $Orgs^{CD}$ barriers were damaged by TNF-α. However, after co-culture with hPMSCs, the intensity of fluorescence in the organoids significantly decreased, indicating that hPMSCs could repair the barrier system of intestinal organoids (Fig. 4G). The results of RT-qPCR, western blotting (WB), and immunofluorescence illustrated that the expression of CLDN1 in the intestinal $Orgs^{CD}$ treated with TNF-α was lower than that of $Orgs^{Health}$, while the expression of CLDN2 was higher. After co-culture with hPMSCs, expression of CLDN1 increased at both the RNA and protein levels while expression of CLDN2 decreased (Fig. 4H–J).

Crypts from the intestines of SAMP1/Yit mice were also successfully extracted (named as $Orgs^{SAMP1}$) and $Orgs^{SAMP1}$ were cultured (Supplementary Fig. 8A). Co-culture with hPMSCs promoted the differentiation and proliferation of $Orgs^{SAMP1}$ and restored $Orgs^{SAMP1}$ barrier functions (Supplementary Fig. 8B–I).

hPMSCs alleviated intestinal inflammation and restored intestinal barrier function via the AMPK-FXR pathway

The mRNA and protein levels of FXR and its downstream target genes small heterodimer partner (SHP) and fibroblast growth factor 19 (FGF19) of $Orgs^{CD}$ treated with TNF-α were lower than that of $Orgs^{Health}$. After co-culture, hPMSC treatment promoted the expression level of FXR and similar results were observed in SAMP1/Yit mice (Fig. 5A, B). In order to discover whether hPMSC treatment could improve the expression of phosphorylation of AMPK (pAMPK) which could regulate the expression of FXR, dorsomorphin (an AMPK inhibitor) and 5-amino-4-imidazolecarboxamide riboside (AICAR; an AMPK activator, as the positive control) were added in the co-culturing system, named as $Orgs^{CD}$ + TNF-α + MSC+Dor group and $Orgs^{CD}$ + TNF-α + AICAR group, respectively. The size and the ratio of secondary to primary $Orgs^{CD}$ were decreased when dorsomorphin was added in a co-cultured system (Fig. 5C, D). FD4 was also added in each group to detect their barrier functions. The intensity of fluorescence in lumen increased in the $Orgs^{CD}$ + TNF-α + MSC+Dor group, while the intensity of fluorescence in the $Orgs^{CD}$ + TNF-α + AICAR group was lower than that in the $Orgs^{CD}$ + TNF-α + MSC+Dor group, indicating that dorsomorphin could prevent hPMSCs to repair the barrier system of intestinal $Orgs^{CD}$. The results of WB and immunofluorescence showed that the expression level of FXR and CLDN1 decreased while CLDN2 increased in the $Orgs^{CD}$ + TNF-α + MSC+Dor group compared with the hPMSC group (Fig. 5D, E). The level of pAMPK was decreased in the $Orgs^{CD}$ + TNF-α group compared with $Orgs^{Health}$ but increased after co-culturing with hPMSCs. However, the expression level of pAMPK was decreased again when dorsomorphin was added in the co-culturing system for 48 h. The mRNA levels of CLDN1, FXR and its downstream target genes SHP and FGF19 in the $Orgs^{CD}$ + TNF-α + MSC+Dor group were lower than that of the hPMSCs group, while the expression level of CLDN2 was higher. Compared with the $Orgs^{CD}$ + TNF-α + MSC+Dor group, the expression levels of CLDN1, FXR, SHP and FGF19 were increased and CLDN2 was decreased in $Orgs^{CD}$ + TNF-α + AICAR group (Fig. 5F). mRNA levels of TNF-α, IL-1β, and IL-6 in $Orgs^{CD}$ + TNF-α + MSC+Dor group were higher than hPMSC group (Supplementary Fig. 9). These results above demonstrated that dorsomorphin could arrest hPMSCs' therapeutic function and hPMSCs alleviated the intestinal inflammation and recovered the intestinal barrier function by activating the AMPK-FXR pathway.

To elucidate the mechanisms of how pAMPK increased the expression of FXR, we examined the recruitment of hepatic nuclear factor-1α (HNF-1α), an upstream transcription factor for FXR to the FXR promoter using chromatin immunoprecipitation (ChIP). As shown in Fig. 5G, the expression level of FXR pulled down with HNF-1α which is associated with FXR promoter, was significantly reduced in $Orgs^{CD}$ treated with TNF-α compared with that in $Orgs^{Health}$ group, but after hPMSCs treatment, the expression level increased. When dorsomorphin was added to the co-culturing system, the level of FXR decreased and the AICAR could counteract the downturn.

hPMSCs-derived IGFBP-4 alleviated intestinal inflammation and restored barrier function by activating AMPK-FXR pathway

hPMSCs culture supernatant was collected and screened for potential therapeutic proteins using antibody arrays for 80 cytokines. The results showed that the top ten cytokines that expressed most were IGFBP-4, IGFBP-3, IGFBP-6, metalloproteinases (TIMP)-2, IGFBP-2, TIMP-1, transforming growth factor beta 1 (TGFb1), vascular endothelial growth factor (VEGF), bone morphogenetic protein (BMP)-5, and IL-6 (Fig. 6A). The expression levels of IGFBP-4 and IGFBP-3 were much higher than other cytokines, which were 119 and 89 ng/mL, respectively, so these two cytokines were selected to find out whether they could activate AMPK-FXR pathway. After adding IGFBP-4 and IGFBP-3 separately for 48 h, the level of pAMPK significantly increased in the IGFBP-4 group while there was no increase in the IGFBP-3 group. The result showed that adding 119 ng/mL IGFBP-4 in the culture system could increase the expression of pAMPK most, compared with other concentrations (Supplementary Fig. 10A). We also detected whether the level of IGFBP4 decreased in CD patients. As shown in Fig. 6B, the level of IGFBP-4 in 90 CD patients was much lower than that in 100 healthy controls.

siRNAs were added to the hPMSCs culture medium to prevent or reduce the expression of IGFBP-4. After transfecting siRNAs for 72 h, green fluorescence could be observed in hPMSCs, indicating that siRNAs had been successfully transfected into hPMSCs (Supplementary Fig. 10B). The expression of IGFBP-4 in the hPMSCs transfected by siRNA3 was much lower than in the control group so we selected siRNA3 for further research (Supplementary Fig. 10C). After co-culturing with hPMSCs transfected by siRNA3, the size and the ratio of secondary to primary $Orgs^{CD}$ were decreased, compared with the $Orgs^{CD}$ + TNF-α + hPMSC group. But the size and the ratio of secondary to primary $Orgs^{CD}$ were increased in the $Orgs^{CD}$ + TNF-α + IGFBP-4 group compared with those in the $Orgs^{CD}$ + TNF-α + hPMSC+siRNA3 group. $Orgs^{Health}$ were used as the control. Then FD4 was used to detect the barrier function of organoids in each group. The results demonstrated that the intensity of green fluorescence in $Orgs^{CD}$ increased in $Orgs^{CD}$ + TNF-α + hPMSC+siRNA3 group compared with that in hPMSC group but the intensity of green fluorescence in $Orgs^{CD}$ was lower in the $Orgs^{CD}$ + TNF-α + IGFBP-4 group than that in $Orgs^{CD}$ + TNF-α + hPMSC+siRNA3 group (Fig. 6C). These results illustrated that IGFBP-4 secreted by hPMSCs could repair the $Orgs^{CD}$ barriers.

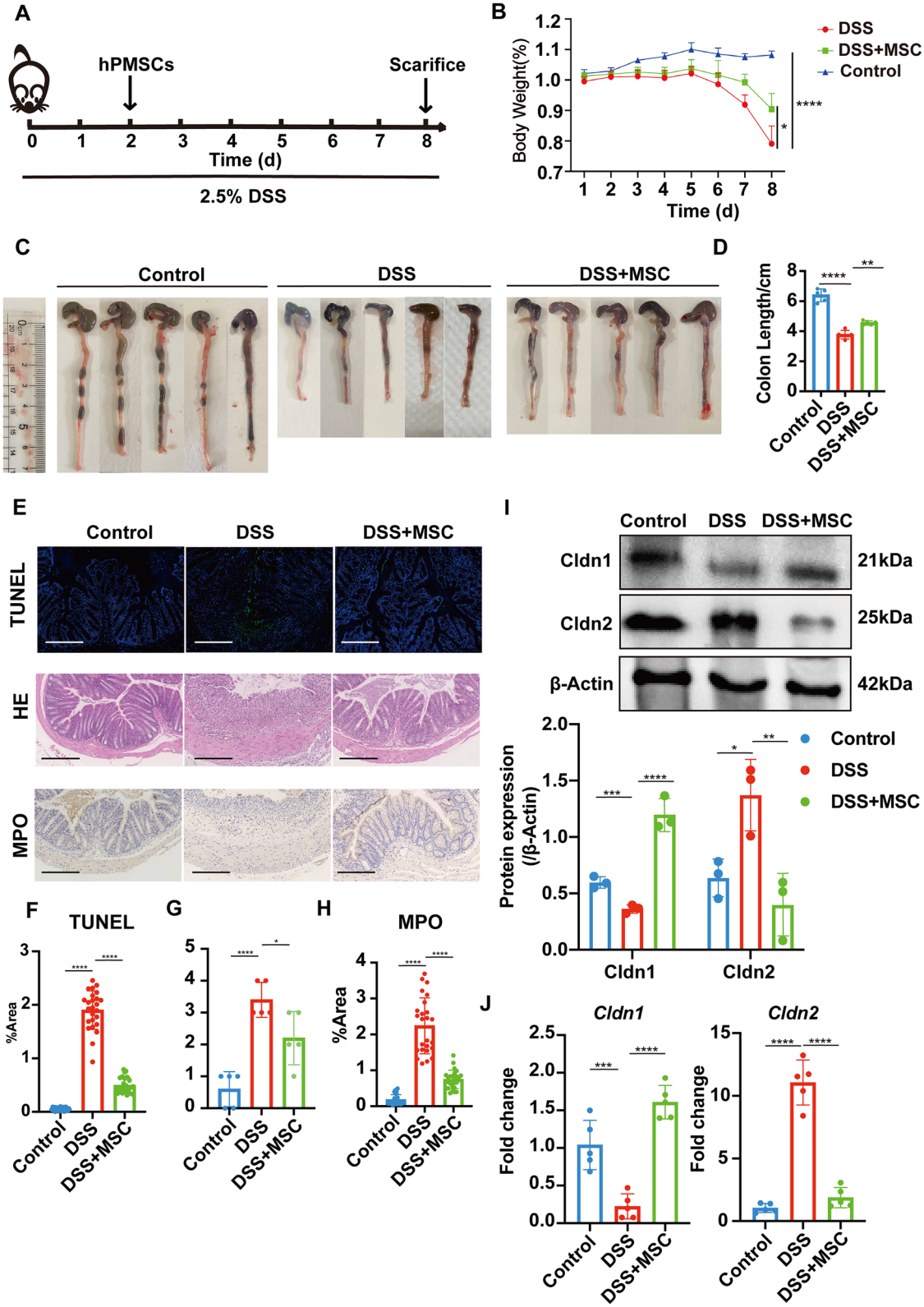

The expressions of pAMPK, FXR and CLDN1 at the protein level of Orgs^{CD} treated with TNF-α co-culturing with hPMSCs transfected by siRNA3, detected by western blotting, were much lower than those of Orgs^{CD} treated with TNF-α co-culturing with hPMSCs and the expression of CLDN2 was contrary. And IGFBP-4 could promote the expression of pAMPK, FXR and CLDN1 and decrease the expression of CLDN2 (Fig. 6D). Then, the expression levels of CLDN1, CLDN2, FXR and its downstream target genes (SHP and FGF19) had the same trend in Orgs^{CD} + TNF-α + hPMSC+siRNA3 group and Orgs^{CD} + TNF-α + IGFBP-4 group (Fig. 6E). These findings were also verified by immunofluorescence (Fig. 6F). Similarly, the expressions of inflammatory factors in Orgs^{CD} + TNF-α + hPMSC+siRNA3 group increased compared with hPMSC group and they dropped in Orgs^{CD} + TNF-α + IGFBP-4 group (Fig. 6G). The result of ChIP showed that the expression of FXR decreased in

Fig. 3 | Therapeutic effects of hPMSCs in a DSS-induced colitis mouse model. **A** Study design for colitis induction and hPMSC transplantation. **B** Body weight curve of control, DSS, and DSS + MSC groups throughout the experiments ($n = 5$ in each group). **C** Gross view of colons for each group ($n = 5$ in each group). **D** Colon length was measured for each group ($n = 3$ in the DSS group; $n = 5$ in the control and DSS + MSC group). **E** Representative TUNEL images (10×, scale bar, 250 μm), H&E images (5×, scale bar, 500 μm), immunohistochemical images of MPO (10×, scale bar, 250 μm) of terminal ileum section of each group. **F** Quantitative analysis of TUNEL (measured in 5 random views per mouse). **G** Histologic scores ($n = 5$ in each group). **H** Positive area of MPO expression. The positive areas of MPO were measured in five random views per mouse for quantitative analysis. **I** WB was performed for Cldn1 and Cldn2 from the colon tissues of each group (experiment performed in triplicate). **J** Gene expression levels of Cldn1 and Cldn2 (five mice in each group). Results were presented as mean ± SD. $^{*}P < 0.05$, $^{**}P < 0.01$, $^{***}P < 0.001$, $^{****}P < 0.0001$. After cell transplantation, body weight loss was slower, colons were longer, colon inflammation was alleviated, the number of infiltrated inflammatory cells and apoptotic cells decreased, and the intestinal barrier was restored.

the $Orgs^{CD}$ + TNF-α + hPMSC+siRNA3 group compared with that in the hPMSC group and the expression of FXR raised in the $Orgs^{CD}$ + TNF-α + IGFBP-4 groups (Fig. 6H).

Discussion

In recent years, with the development of regenerative medicine, MSCs have been used to treat inflammatory diseases because of their low immunogenicity and immunosuppressive effects. MSCs can suppress the proliferation and activation of T cells (both $CD4^+$ T cells and $CD8^+$ T cells) and B cells, except for inducing their apoptosis by strongly attaching to cells through their adhesion molecules[34–37] or producing soluble factors such as TGF-β, hepatocyte growth factor (HGF), indoleamine 2,3-dioxygenase (IDO), prostaglandin E2 (PGE2), and IL-6[38–40]. Additionally, MSCs can induce the aggregation and proliferation of Treg cells which exert immunomodulatory and anti-inflammatory effects through an HLA-G5-dependent pathway regulated by PGE2, TGF-β1, which is secreted by MSCs. MSCs can transfer T cells from the canonical NF-κB pathway to the non-canonical one, and this group of cells would highly express the immunosuppressive marker CD69[41,42]. Expect reducing B cell proliferation, MSCs could secrete IL-1RA and CCL2 to inhibit the maturation and immunoglobulin antibodies production of B cells[39,40]. MSCs can also regulate the activity of natural killer cells, the polarization of macrophages, and the immune response[43]. Additionally, MSCs can preferentially target damaged tissues guided by chemotactic signals released at the injury site, then secret some cytokines, such as HGF and tumor necrosis factor-stimulated gene 6 (TSG-6), or exosomes to exert their therapy effects on the intestinal inflammation, intestine integrity and intestinal fibrosis[44–48]. Intriguingly, MSCs undergo apoptosis and produce lots of apoptotic vesicles (apoVs) after in vivo application, which could be removed by macrophages, known as efferocytosis[43,49,50]. The efferocytosis of apoVs induced transcriptional reprogramming of macrophages in vitro and generated imperative immunosuppressive effects via actively eliciting anti-inflammation responses in macrophages[51,52].

MSCs can be obtained from different tissues, including bone marrow, umbilical cord, adipose, and tooth tissue[53–57]. Those derived from the placenta can be obtained noninvasively. A large number of high-quality MSCs can be extracted from a placenta obtained at term delivery, and many studies have shown that these MSCs have equal or better therapeutic potential than MSCs derived from human bone marrow or the umbilical cord[58–60].

There have been many clinical studies on the treatment of CD with MSCs, although the results of many have been unsatisfactory. CD patients receiving MSC therapy have relapsed many times and experienced worsened conditions; some have required surgical intervention[61–63]. Previous reports have lacked a complete preclinical evaluation. To provide a reference for clinical use, a series of preclinical evaluations of the safety and effectiveness of hPMSC transplantation were conducted.

Our data showed that following hPMSC injection into AKR/J and SCID mice, no tumors were observed in any organs, indicating that hPMSCs have no obvious tumor formation potential. In addition, hPMSCs could not be implanted for a long time which could disappear around day 21 in vivo and mainly concentrated at inflammatory sites. We found no evidence that hPMSCs could transform into intestinal epithelial cells or other intestinal cells. We did not observe any abnormalities in terms of general, blood biochemical, and pathological aspects, suggesting that hPMSC transplantation did not cause toxicity. At the same time, the number of Treg and the ratio of $CD4^+/CD8^+$ T cells in the spleens of mice after transplantation did not change. The levels of inflammatory factors TNF-α, IL-1β, and IL-6 in the terminal ileum were not abnormally increased. These results suggested that the human body is not likely to have an abnormal immune response to hPMSC transplantation and hPMSCs have good safety and clinical potential.

A number of animal models of IBD have been developed to investigate the causes of CD and ulcerative colitis (UC)[64]. However, there is no single animal model that represents all pathogenic and clinical features of human IBD. Nevertheless, each animal model has its characteristics, which gives us a unique chance to understand the mechanisms of chronic intestinal inflammation. The SAMP1/Yit mouse, a senescence-accelerated mouse (SAM) strain derived from AKR/J mice, is an appropriate model to investigate the etiopathogenetic mechanisms of CD[65], because intestinal inflammation in this model is truly spontaneous, without the need for genetic, chemical, or immunological manipulation that closely resembles human CD, including segmental and transmural chronic inflammation of the terminal ileum and in some cases, perianal fistulae[66]. SAMP1/Yit mice exhibit some intestine epithelial barrier dysfunction as a primary defect, which results in immunological responses and immune cell infiltration in the ileum[67].

To test the therapeutic effect of hPMSCs in CD mouse models, hPMSCs were injected into two CD mouse models, SAMP1/Yit mice and DSS-induced acute colitis mice. Therapeutic effects of hPMSC transplantation were demonstrated by both mouse models. The results also matched the previous results of clinical trials and meta-analyses about stem cell treatment for liver diseases and CD[16,68–70].

Organoid technology can effectively expand intestinal epithelial tissue derived from CD patients in vitro, and cultured organoids have CD characteristics and can proliferate, undergo apoptosis, differentiate, and contribute to barrier formation. Compared to two-dimensional cell lines, organoids can better simulate the disease state and provide a better evaluation platform for the study of the effectiveness of hPMSC transplantation for CD in vitro. In a co-culture system of organoids and hPMSCs, hPMSCs increased organoid volume, reduced apoptotic cells, and restored organoid barrier function. Overall, our results suggested that hPMSCs are effective for CD treatment.

Although the development of intestinal inflammation in CD patients is multifactorial, recent research has shown that a decrease in FXR expression leads to a decrease in barrier function and intestinal inflammatory infiltration in such patients[71,72]. Previous studies have shown that decreased expression of the bile acid receptor FXR in the intestines of IBD patients results in bile acid metabolism disorders, causing serious intestinal inflammation[30,31]. At the same time, deletion of the FXR can also lead to impairment of barrier function in mice[73]. Our results confirm that in the intestines of SAMP1/Yit mice, expression levels of the FXR and its downstream target genes are all decreased, intestinal muscularis propria is infiltrated by immune cells and barrier function is damaged and hPMSCs could ameliorate the above phenotypes. Some studies have suggested that phosphorylation of AMPK can activate FXR in the liver and kidney, but the relationship between AMPK and FXR in the intestine has not been evaluated. Our results showed that the level of pAMPK of $Orgs^{CD}$ is lower than healthy control and hPMSCs could increase the level of pAMPK which could improve the expression of FXR, then alleviate intestinal inflammation and recover intestinal barrier function.

IGFBP-4 is a kind of cytokine that is highly expressed in the female reproductive system and liver. So MSCs from placenta and umbilical cord can highly secret this cytokine than MSCs from other tissues. It is reported

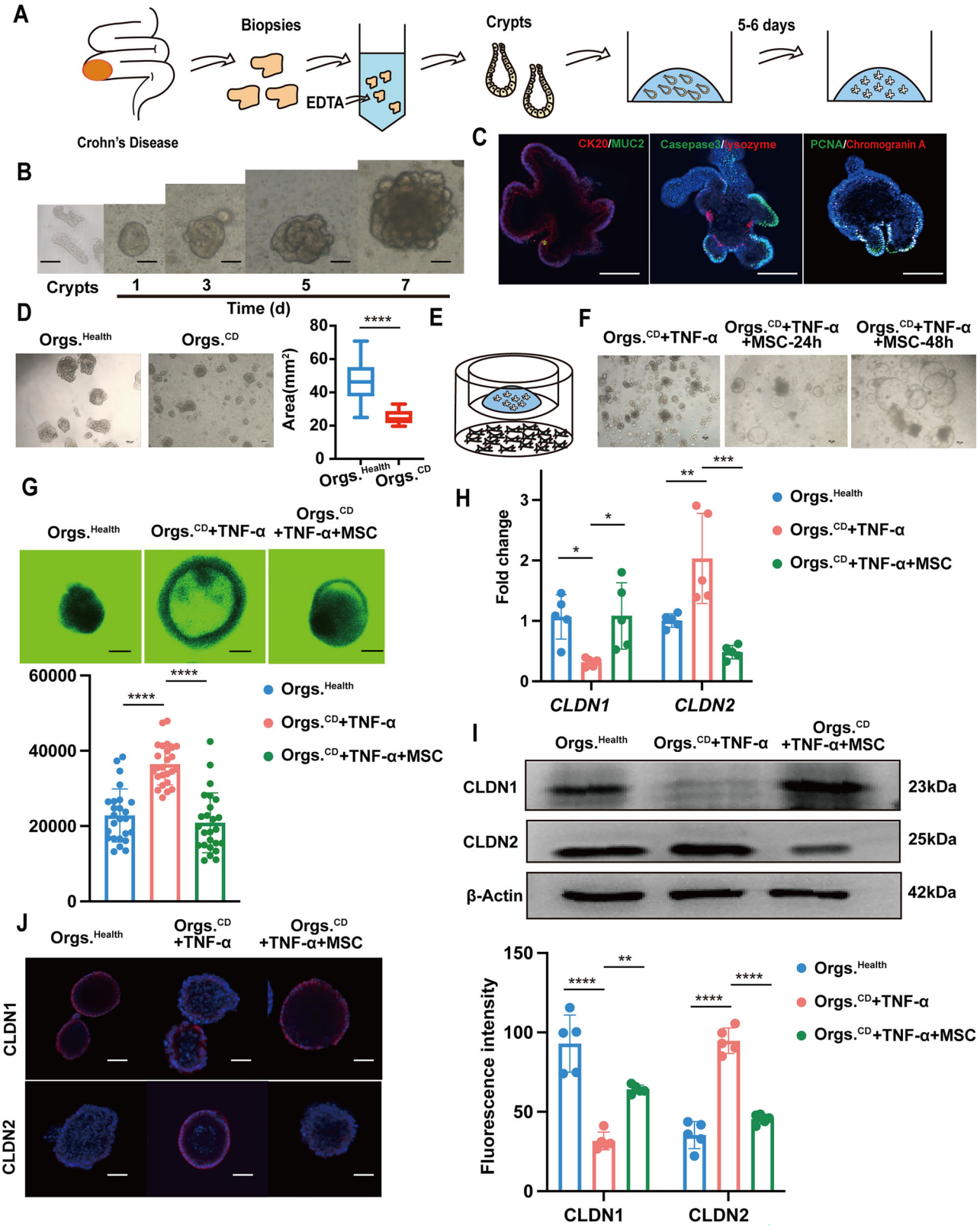

that IGFBP-4 plays an important role in cell proliferation, differentiation, and senescence. IGFBP-4 is required for adipogenesis, skeletal growth, and cardiomyocyte differentiation[25,74–76]. IGFBP-4 could also attenuate lung cancer, osteosarcoma, metastasis of intrahepatic cholangiocarcinoma, and hepatic carcinogenesis[77–79]. Yet the relationship between IGFBP-4 and CD is still unknown. Our results showed that the level of IGFBP-4 in CD patients' serum was much lower than in healthy control which indicated that the shortage of IGFBP-4 might be associated with CD. The results of further research found that IGFBP-4 secreted by hPMSCs could alleviate intestinal inflammation and repair intestinal barrier function by improving the expression of CLDN1 and decreasing the expression of CLDN2 in vitro. IGFBP-4 might be a potential therapeutic cytokine for CD.

Fig. 4 | hPMSCs promoted proliferation and restored barrier function of Orgs^{CD}. **A** Crypts were extracted from biopsies or tissues removed by surgery and intestinal organoids were cultured. **B** Representative images of cultured intestinal organoids (10×, scale bar, 100 μm). **C** Representative immunofluorescence images of CK20, MUC2, Caspase 3, lysozyme, PCNA, and Chromogranin A of organoids (20×, scale bar, 100 μm). **D** Representative bright field images (4×, scale bar, 100 μm) and the size of intestinal Orgs^{health} and Orgs^{CD} (at least 25 organoids from three patients and three health controls respectively in each group). **E** In the co-culture system, Orgs^{CD} treated with TNF-α were cultured in the transwell and hPMSCs were cultured in the lower level. **F** Representative bright field images (4×, scale bar, 50 μm) of intestinal Orgs^{CD} treated with TNF-α, and Orgs^{CD} treated with TNF-α co-cultured with hPMSCs for 24 and 48 h. **G** Orgs^{Health} and Orgs^{CD} cultured for 5 days were treated with TNF-α, or TNF-α + hPMSCs for 48 h, and FITC-dextran 4 (FD4) flux across the organoid epitheliums normalized to the surface area of organoids was measured (40×, scale bar, 50 μm). Orgs^{health} were used as the control (a total of 25 organoids were calculated from three independent experiments in each group). **H** Gene expression levels of CLDN1 and CLDN2 (five independent experiments). **I** WB of CLDN1 and CLDN2 from organoids of each group (experiment performed in triplicate). **J** Representative immunofluorescence for CLDN1 and CLDN2 (20×, scale bar, 100 μm). Five organoids were calculated in each group. Results were presented as mean ± SD. $^{*}P < 0.05$, $^{**}P < 0.01$, $^{***}P < 0.001$, $^{****}P < 0.0001$. Co-culture with hPMSCs promoted Orgs^{CD} proliferation and restored Orgs^{CD} barrier functions disrupted by TNF-α.

Overall, our results showed that hPMSCs are safe and therapeutically effective for SAMP1/Yit and DSS-induced colitis mice and intestinal organoids derived from CD patients. We found that IGFBP-4 secreted by hPMSCs could activate the AMPK-FXR pathway to alleviate intestinal inflammation and repair intestinal barrier function.

Methods

Cell preparation

hPMSCs were obtained from the Cell Bank of State Key Laboratory for the Diagnosis and Treatment of Infectious Diseases, Zhejiang University. hPMSCs used in this study were derived from the villous trophoblast portion of the placenta. Additionally, hPMSCs used in the in vitro experiments were all sourced from the same individual. hPMSCs surface marker expression was analyzed by flow cytometry and hPMSC features were investigated by adipogenic, osteogenic, and chondrogenic differentiation assays[80,81]. hPMSCs in passages 3 to 5 were used. Details were provided in the Supplementary Information. Studies were approved by the Clinical Research Ethics Committee of The First Affiliated Hospital of Zhejiang University School of Medicine and in accordance with the Declaration of Helsinki.

Animals

C57/BL6 and SCID mice were purchased from Ziyuan Laboratory Animal Science and Technology Co. (Ltd., Hangzhou, China), and SAMP1/Yit and control AKR/J mice were from the Jackson Laboratory (Bar Harbor, ME, USA). All animals were housed in ventilated cages under controlled temperature (18–25 °C), humidity (30–70% RH), and normal light/dark (12/12 h) cycle conditions in the Laboratory Animal Center of The First Affiliated Hospital of Zhejiang University School of Medicine. All the mice were measured by a random order and the cages were randomly allocated to minimize potential confounders. During the experiment, the personnel handling the mice were aware of the group allocation in order to apply the appropriate treatment. Efforts were made to maintain blinding during the outcome assessment and data analysis stages to reduce subjective bias. In the end, all mice were sacrificed with CO_2. All animal experimental procedures were conducted according to the Animal Research: Reporting of In Vivo Experiments (ARRIVE) guidelines and were authorized by approved by the Animal Experimental Ethical Inspection of The First Affiliated Hospital of Zhejiang University School of Medicine. We have complied with all relevant ethical regulations for animal use.

Preparation and identification of intestinal organoids from human and mouse models

1 cm^2 inflammatory intestinal tissues of CD patients obtained from surgical resection and one biopsy of health controls collected during endoscopy were used to isolate crypts. 4 cm small intestines above the ileocecal valve from SAMP1/Yit and AKR/J mice were collected to isolate crypts and culture[82,83]. Briefly, fresh intestinal or biopsy tissues were harvested in ice-cold phosphate-buffered saline (PBS) containing antibiotics (1% penicillin/streptomycin; Gibco, Grand Island, NY, USA). Crypts were isolated by adding 2 mM ethylene diamine tetraacetic acid (EDTA; Sangon Biotech, Shanghai, China) for 60 min at 4 °C. Then the tissues were transferred to ice-cold PBS followed by vigorous mechanical disruption. The supernatant with crypts was centrifuged by 450 × g at 4 °C. Then the crypts were suspended in growth factor-reduced phenol-red free Matrigel (Corning, Bedford, MA, USA), transferred to 24-well plates (Thermo Fisher Scientific, Waltham, MA, USA), and incubated at 37 °C with 5% CO_2 for 10 min to polymerize the Matrigel. The crypts were overlaid with 500 μL human or mouse IntestiCult™ organoid growth medium (STEMCELL Technologies Inc., Vancouver, Canada) per well and maintained at 37 °C in a 5% CO_2/air mix. The culture medium was refreshed every 3 days, and organoids were passaged every 6–7 days. Organoids in passages 3 to 5 were used in further experiments. This study was carried out in accordance with Declaration of Helsinki and approved by the Clinical Research Ethics Committee of The First Affiliated Hospital of Zhejiang University School of Medicine (Reference number: 2021-158).

To identify what we cultured were intestinal organoids, the fluorescence staining of organoids cultured for 7 days was conducted[35,36]. Details were provided in the Supplementary Information.

Safety evaluation

Twenty-four-week-old male SAMP1/Yit mice and age-matched male AKR/J mice were used to evaluate the safety of hPMSC transplantation by intraperitoneal infusion. The hPMSC dose was 2×10^6 cells in 200 μL PBS.

Acute toxicity. A cage of AKR/J mice were injected with hPMSCs or 200 μL PBS, respectively ($n = 5$ in each group). After 1 week, body and organ weight were measured, the organ coefficient (organ weight/mouse weight on the day of dissection ×100%) was calculated and peripheral blood serum, terminal ileums, livers, and kidneys were collected for follow-up analysis.

Long-term toxicity. A cage of AKR/J mice were injected with hPMSCs or 200 μL PBS, respectively ($n = 5$ in each group). Body weight and general conditions were continuously recorded for 8 weeks. Organ weight was determined and peripheral blood serum, terminal ileums, livers, and kidneys were collected for follow-up analysis.

Abnormal immune response. A cage of AKR/J mice were injected with hPMSCs or 200 μL PBS, respectively ($n = 3$ in each group). After 1 week, spleens were collected. Immune cells in the spleen were extracted and the ratios of spleen regulatory T cells (Treg) cells and $CD4^+/CD8^+$ T cells were analyzed. Terminal ileum tissue of mice (8 cm up from the ileocecal valve) was collected and RNA was extracted to analyze the inflammatory factors TNF-α, IL-6, and IL-1β.

Biological distribution. DiR-labeled (Invitrogen, Carlsbad, CA, USA) hPMSCs were injected into a cage of SAMP1/Yit and a cage of AKR/J mice ($n = 4$ in each group), and the distribution and survival of hPMSCs in vivo were imaged on an IVIS Spectrum (PerkinElmer, Waltham, MA, USA). On the third day after injection, the abdominal organs of the mice were dissected out. The distribution of DiR fluorescence was observed using the IVIS system, and frozen sections of the intestinal terminal sections (8 cm up from the ileocecal valve) were observed by fluorescence inverted microscope (Carl Zeiss, Germany).

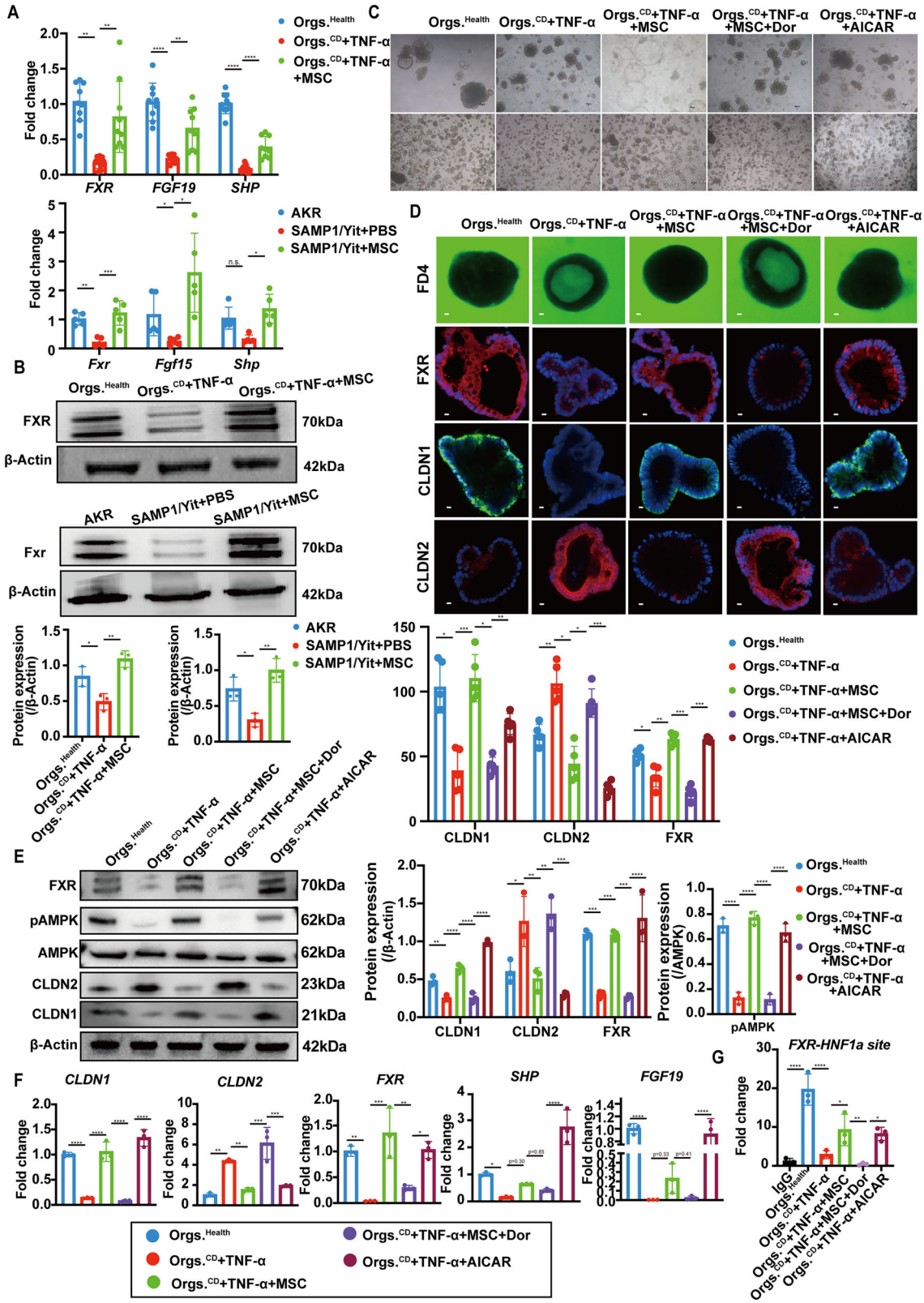

Oncogenicity. SCID mice and AKR/J mice were both used for the evaluation of oncogenicity. hPMSCs or 200 μL PBS were injected into AKR/J mice and SCID mice and all mice were weighed weekly. Mice were observed continuously for potential tumor formation ($n = 5$ in each group).

Evaluation of effectiveness

Evaluation of effectiveness in mouse models. SAMP1/Yit mice and C57/BL6 mice fed DSS were used in the following experiment. 2×10^6 hPMSCs in 200 μL PBS were intraperitoneally injected into a cage of SAMP1/Yit mice. A cage of age-matched male AKR/J mice served as

Fig. 5 | hPMSCs alleviated intestinal inflammation and repaired barrier function via AMPK-FXR pathway activation. A Upper graph: Expression levels of FXR mRNA and downstream genes FGF19 and SHP in intestinal $Orgs^{health}$, $orgs^{CD}$ + TNF-α, and following co-culture with hPMSCs for 48 h (data were generated from three independent experiments per subject and 3 subjects in each group). Bottom graph: mRNA levels of FXR, FGF19, and SHP in terminal ileum tissues of AKR/J mice and SAMP1/Yit mice injected with or without hPMSCs ($n = 5$ in each group). **B** Upper graph: Representative WB and relative expression levels of FXR intestinal $Orgs^{health}$, $Orgs^{CD}$ + TNF-α, and following co-culture with hPMSCs for 48 h (experiment performed in triplicate). Bottom graph: Representative WB of FXR in terminal ileum tissues of AKR/J mice and SAMP1/Yit mice injected with or without hPMSCs (experiment performed in triplicate). **C** Upper panel: Representative images of $Orgs^{health}$, $Orgs^{CD}$ + TNF-α, $Orgs^{CD}$ co-culturing with hPMSCs ($Orgs^{CD}$+TNF-α + MSC), $Orgs^{CD}$ treated with TNF-α co-culturing with hPMSCs and dorsomorphin ($Orgs^{CD}$ +TNF-α + MSC+Dor) and co-culturing with AICAR ($Orgs^{CD}$+TNF-α + AICAR), respectively (4×, scale bar, 50 μm). Bottom panel: Representative pictures of secondary organoids from each group culturing for 7 days after passage (4×, scale bar, 50 μm). **D** Representative immunofluorescence images for FD4, FXR, CLDN1, and CLDN2 of each group (40×, scale bar, 10 μm). **E** WB of FXR, pAMPK, AMPK, CLDN1, and CLDN2 protein from organoids of each group (experiment performed in triplicate) normalized to β-actin and correspondence quantification **F** Gene expression levels of CLDN1, CLDN2, FXR, SHP, and FGF19 (three independent experiments in each group). **G** The association of HNF-1α with HNF-1α binding site on the promoter of FXR in each group (three independent experiments in each group). Results were presented as mean ± SD. $^{*}P < 0.05$, $^{**}P < 0.01$, $^{***}P < 0.001$, $^{****}P < 0.0001$. hPMSCs increased pAMPK in $Orgs^{CD}$ treated with TNF-α and the terminal ileum of SAMP1/Yit mice, thereby increasing the association of HNF-1α with HNF-1α binding site on the promoter of FXR, then activating FXR, promoting alleviation of inflammation, and repair of barrier function.

controls and which injected with 200 μL PBS. Five mice were allocated in each group mentioned above. Mice were sacrificed 1 week after the injection. Intestines about 8 cm up from the ileocecal valve were collected for later analysis.

Six- to eight-week-old male C57/BL6 mice were randomly divided into three groups according to the drawing lots method to allocate the mice to PBS group (Control), 2.5% DSS treatment group (DSS), and 2.5% DSS + hPMSC transplantation group (DSS + MSC) in turn ($n = 5$ in each group). Mice in the DSS and DSS + MSC groups were fed 2.5% DSS (36–50 kDa; MP Biomedical, Solon, OH, USA) (w/v) in drinking water from day 0 to day 8 to establish the acute colitis model; mice in the PBS group received normal drinking water. Body weights were measured every day throughout the experiment. On the second day of DSS feeding, mice in the DSS + MSC group were intraperitoneally injected with 2×10^6 hPMSCs in 200 μL PBS. Mice in the other two groups were injected with 200 μL PBS. On day 8, all mice were sacrificed with CO_2 and colons from the cecum to the anus were collected and measured.

Evaluation of effectiveness in organoids. $Orgs^{CD}$ and $Orgs^{SAMP1}$ were used as cell models to evaluate the effectiveness of hPMSCs in vitro. $Orgs^{Health}$ and intestinal organoids from AKR/J mice (named as $Orgs^{AKR}$) were used as controls. To establish organoid-hPMSC coculture system, intestinal organoids embedded in Matrigel were plated on the inner chamber of polyester transwell inserts (0.4 μm pore size, Corning). On day 3–4 after plating, 60 ng/mL TNF-α was added in the $Orgs^{CD}$ to stimulate organoids as inflammatory status, then co-cultured for 48 h with hPMSCs which were at 80% confluence in the bottom chambers of the transwell plate[84]. The culture medium was removed, 300 μL cell recovery solutions (Corning, Bedford, MA, USA) were added to each well to collect organoids, and the wells were placed on ice and incubated for 30 min to free the organoids. The organoids were used for RNA and protein extraction, immunofluorescence staining, and permeability measurements.

To measure the permeability of intestinal organoids, $Orgs^{CD}$ and $Orgs^{Health}$ of the same passage were plated in transwells. After 3–4 days of culture, 60 ng/mL TNF-α was added to the $Orgs^{CD}$ culture medium. Then, hPMSCs were co-cultured with $Orgs^{CD}$ for 48 h; $Orgs^{Health}$ were co-cultured with hPMSC culture medium for 48 h. After freeing the organoids in each well by cell recovery solution, organoids were transferred to culture medium containing 0.1 mg/mL FD4 (Sigma Aldrich, St. Louis, MO, USA) and incubated at 37 °C with 5% CO_2 for 2 h. Images of each organoid were captured by a confocal microscope (LSM700, Carl Zeiss, Germany) and the fluorescence intensity of each organoid was calculated with ImageJ software (NIH, Bethesda, MD, USA).

In order to find out whether hPMSCs could regulate pAMPK, 0.1 μM dorsomorphin (MedChemExpress, New Jersey, USA), as the AMPK inhibitor, was added in the hPMSC-$Orgs^{CD}$ (treated with TNF-α) co-culturing system and cultured for 48 h. 0.25 nM AICAR (MedChemExpress, New Jersey, USA), as the AMPK activator, was added in the $Orgs^{CD}$ (treated with TNF-α) and cultured for 48 h as the positive control.

To explore the role of IGFBP-4, short interfering RNA (siRNA, 50 nmol/L) of IGFBP-4 and negative control siRNA were used to transfect hPMSCs to prevent or reduce the expression of IGFBP-4. 72 h after transfection, hPMSCs were co-cultured with $Orgs^{CD}$ (treated with TNF-α) for 48 h. Then the $Orgs^{CD}$ were collected for further analysis.

Blood biochemistry analysis

Serum samples of mice were used to assess liver, renal and lipid metabolism function using alanine aminotransferase (ALT), aspartate aminotransferase (AST), albumin (ALB), total bile acid (TBA), total bilirubin (TBIL), blood urea nitrogen (BUN), creatinine (CRE), lactate dehydrogenase (LDH), triglyceride (TG), and total cholesterol (TCHO) kits (Jiancheng, Nanjing, China), according to the manufacturer's instructions.

Serum samples were collected from 90 CD patients and 100 healthy controls treated in The First Affiliated Hospital of Zhejiang University School of Medicine, using human insulin-like growth factors binding protein 4 (IGFBP-4) ELISA Kit (Mskbio, Wuhan, China) to assess IGFBP-4, according to the manufacturer's instruction.

Histology, immunostaining, and TUNEL analyses

Histology of the colon, terminal ileum, liver, and kidneys was performed as follows. Briefly, the tissues were fixed in 4% paraformaldehyde and embedded in paraffin the following day. Tissue sections were stained with hematoxylin and eosin (H&E) to assess pathological changes. Intestinal villus height, muscularis propria, and submucosal thickness per mouse were measured in five random views and the average was calculated for quantitative analysis. A score was given in a blinded fashion by an independent observer as per the severity of pathology[85].

Immunohistochemical staining was performed using anti-MPO polyclonal antibody (dilution, 1:1000; EPR20257 Abcam, Cambridge, MA, USA), anti-Ly6G (dilution, 1:200; RB6-8C5, Abcam), anti-α-SMA polyclonal antibody (dilution, 1:500; 1A4, Abcam), anti-CLDN1 monoclonal antibody (dilution, 1:50; A-9, Santa Cruz Biotechnology, Santa Cruz, CA, USA), anti-CLDN2 monoclonal antibody (dilution, 1:100, 12H12, Thermo Fisher Scientific), anti-S100A8 (dilution, 1:1000; EPR3554, Abcam) and anti-S100A9 (dilution, 1:1000; EPR22332-75, Abcam). TUNEL staining was performed using a TUNEL BrightGreen Apoptosis Detection Kit (Vazyme, Nanjing, China) according to the manufacturer's instructions. The positive areas of MPO were measured in five random views per mouse for quantitative analysis.

The fluorescence staining of organoids was performed using anti-PCNA primary monoclonal antibody (dilution, 1:200; PC10, Abcam), anti-Caspase 3 primary monoclonal antibody (dilution, 1:250; 74T2, Thermo Scientific), anti-CK20 primary monoclonal antibody (dilution, 1:200; EPR1622Y, Abcam), anti-MUC2 primary monoclonal antibody (dilution, 1:50; Ccp58, Santa Cruz), anti-lysozyme monoclonal primary antibody (dilution, 1:250; EPR2994(2), Abcam) and anti-Chromogranin A polyclonal primary antibody (dilution, 1:200; RM1025, Abcam). After

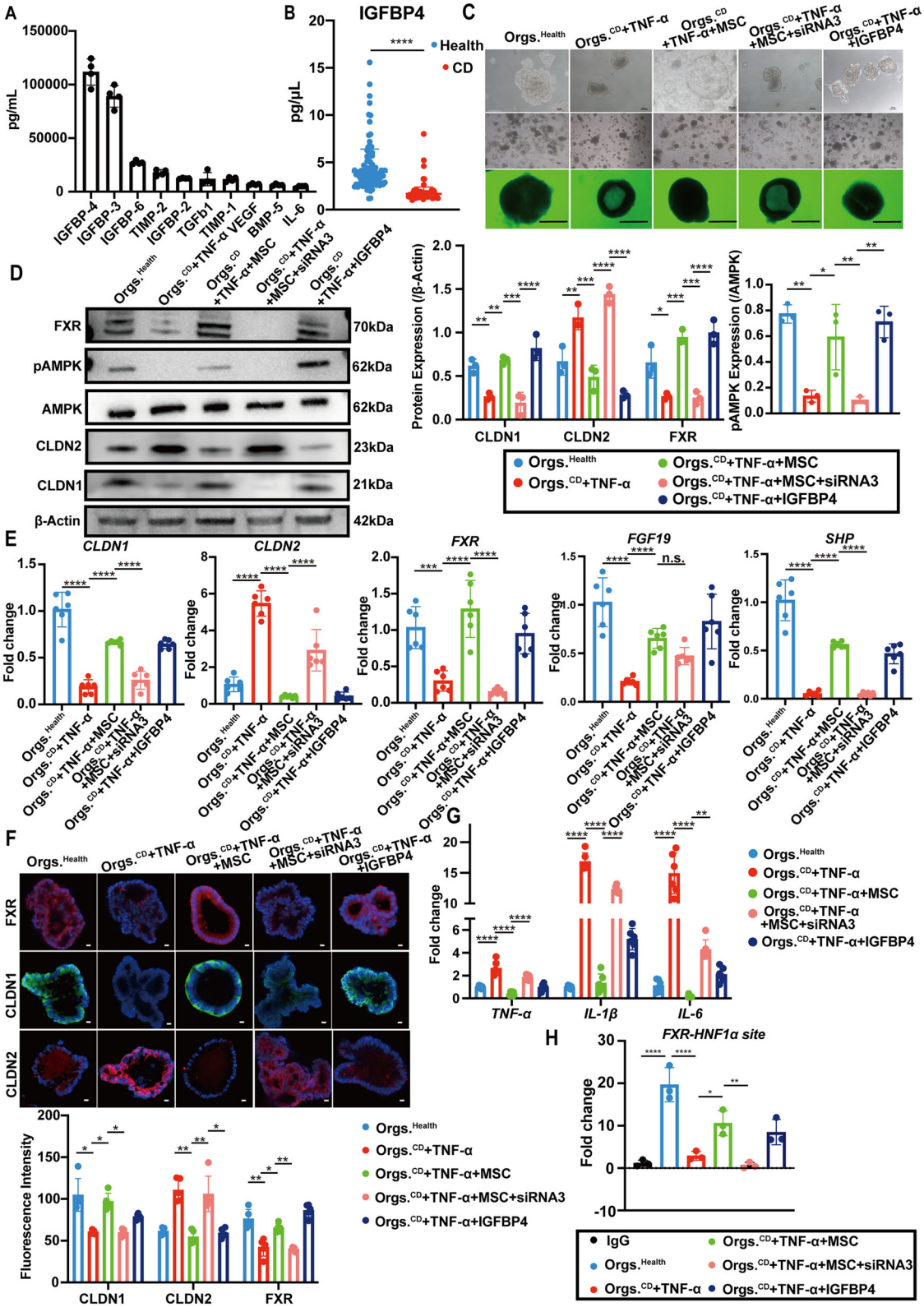

incubating with Alexa Fluor 488 rabbit anti-mouse secondary antibody (dilution, 1:200, Abcam), Alexa Fluor 647 rat anti-rabbit secondary antibody (dilution, 1:200, Abcam), and DAPI (dilution, 1:200, Abcam), the organoids could transfer to a confocal dish and detected by confocal microscope (LSM700, Carl Zeiss, Germany). Details were provided in the Supplementary Information.

Extraction and detection of whole immune cells in the spleen

Mouse spleens were ground in PBS containing 0.1% bovine serum albumin (BSA), and the suspension was filtered using a 70 μm strainer. After centrifugation at 400 × g for 5 min, 5 mL ammonium chloride-potassium (ACK) lysis buffer (Gibco, USA) was added to the precipitates. After incubation at room temperature for 8 min, PBS containing 0.1% BSA was added,

Fig. 6 | hPMSCs-derived IGFBP-4 alleviated intestinal inflammation and repaired barrier function via AMPK-FXR pathway. **A** The top ten cytokines that hPMSCs secreted most (4 independent experiments). **B** The levels of IGFBP-4 in the serum of 90 CD patients and 100 healthy controls. **C** Upper panel: Representative images of $Orgs^{health}$; $Orgs^{CD}$ + TNF-α; $Orgs^{CD}$ + TNF-α co-culturing with hPMSCs, hPMSCs transinfected by siRNA3, and IGFBP-4, respectively (10×, scale bar, 100 μm). Middle panel: Representative pictures of secondary organoids from each group culturing for 7 days after passage (4×, scale bar, 50 μm). Bottom panel: Representative immunofluorescence images for FD4 in each group (40×, scale bar, 50 μm). **D** WB of FXR, pAMPK, AMPK, CLDN1, and CLDN2 from organoids of each group (experiment performed in triplicate) normalized to β-actin and correspondence quantification. **E** Gene expression levels of CLDN1, CLDN2, FXR, SHP, and FGF19 (5 independent experiments in each group). **F** Representative immunofluorescence images for FXR, CLDN1, and CLDN2 (40×, scale bar, 10 μm) in each group. **G** Gene expression levels of TNF-α, IL-6, and IL-1β (5 independent experiments in each group). **H** The association of HNF-1α with HNF-1α binding site on the promoter of FXR in each group (three independent experiments in each group). Results were presented as mean ± SD. *$P < 0.05$, **$P < 0.01$, ***$P < 0.001$, ****$P < 0.0001$. IGFBP-4 was the cytokine that hPMSCs secreted most and the level of IGFBP-4 in CD patient serums was much lower than the healthy controls. IGFBP-4 could activate the AMPK-FXR pathway and then promote the alleviation of inflammation and repair of barrier function. However, hPMSCs secreted lower levels of IGFBP-4 could not play such a therapeutic role.

and the supernatant with immune cells was filtered through a 70 μm strainer and centrifuged at 400 × g for 5 min at 4 °C. The immune cells found in the precipitate were stained with FVS780, FITC-conjugated anti-mouse CD45 (Clone: 30-F11), APC-conjugated anti-mouse CD3 (Clone: 145-2C11), PE-conjugated anti-mouse CD4 (Clone: GK1.5), Percp cy5.5-conjugated anti-mouse CD8 (Clone: 53-6.7), BV510-conjugated anti-mouse CD25 (Clone: 3C7), and BV421-conjugated anti-mouse Foxp3 (Clone: MF23) (BD, San Diego, CA, USA) successively. Data were acquired via the CytoFLEX LX Flow Cytometer (Beckman Colter, Inc., Brea, CA, USA).

Measurement of mouse intestine permeability

The intestinal permeability assay in vivo was performed[86]. Mice were fasted for 4 h before being gavaged with FD4 (600 mg/kg body weight) in PBS. After 4 h, blood samples were harvested. Fluorescent intensity in the plasma was measured at 485/525 nm using a SpectraMax M5/M5e microplate reader (Molecular Devices, San Jose, CA, USA).

ChIP analysis

ChIP analysis was performed as described by the manufacturer (Beyotime, Shanghai, China). Briefly, organoids in each group were freed by cell recovery solution and perfused with 1% paraformaldehyde in culture medium at 37 °C to cross-link protein-DNA complexes for 10 min. Then glycine solution was added to stop the cross-linking. The cross-linked chromatin was cut by MNase for immunoprecipitation with the polyclonal antibodies against HNF-1α (EPR23054-108, Abcam), or normal rabbit immunoglobulin G (IgG). DNA fragments were analyzed by quantitative polymerase chain reaction (q-PCR) using primers flanking indicated promoter regions.

Cytokine antibody array

hPMSCs were inoculated at a density of 2×10^5 cells per well into a 6-well plate. After 24 h, PBS was used to wash the cells twice and MEM containing 2% FBS was added for cultivation. The culture medium was collected after 48 hours of cultivation ($n = 4$). Quantibody® Human Cytokine Antibody Array 640 (QAH-CAA-640) was used to measure the relative levels of 80 cytokines according to protocols in the user manual.

Quantitative RT-PCR

For reverse transcription, total RNA from mouse tissues or organoids was isolated with TRIzol® reagent (Invitrogen, Carlsbad, CA, USA) according to the manufacturer's instructions. RNA (1 μg) was reverse transcribed into cDNA using HiScript II Q RT SuperMix (R223-01; Vazyme). qPCR was performed and analyzed using ABI QuantStudio-5 (Applied Biosystems, Waltham, MA, USA). SYBR Green Supermix (Thermo Fisher Scientific) was used for quantitative assessment of target mRNA levels; β-actin was used as a housekeeping gene to normalize total RNA. The sequences of forward and reverse primers are shown in Supplementary Table 1.

Western blotting analysis

Organoids and tissues were lysed in RIPA lysis buffer (Beyotime Biotech Co., Ltd., Shanghai, China) with proteinase and phosphatase inhibitors (Sigma Aldrich). Protein concentration in the supernatant was measured with a BCA protein assay kit (Beyotime Biotech Co., Ltd.). Sodium dodecyl sulfate-polyacrylamide gel electrophoresis (SDS-PAGE, 12%) was used to separate proteins, and proteins were transferred to a polyvinylidene difluoride membrane. The blots were incubated with the following primary antibodies: anti-CLDN1 monoclonal antibody (dilution, 1:1000; A-9, Santa Cruz), anti-CLDN2 monoclonal antibody (dilution, 1:1000; 12H12, Thermo Fisher Scientific), anti-FXR monoclonal antibody (dilution, 1:1000; EPR7932, Abcam), anti-AMPK alpha 1 monoclonal antibody (dilution, 1:1000; D5A2, Cell signaling technology, Danvers, MA, USA), anti-pAMPK alpha 1 monoclonal antibody (dilution, 1:1000; 40H9, Cell signaling technology), and anti-β-actin monoclonal antibody (dilution, 1:1000; AC-15, Abcam). Blots were visualized and digitally scored with a ChemiScope Western Blotting Imaging System (Clinx Science Instruments Co., Ltd., Shanghai, China). ImageJ software was used to analyze images.

Statistics and reproducibility

All data were expressed as mean ± SD. Statistical analysis was performed using GraphPad Prism 7 software (GraphPad Software, Inc., La Jolla, CA, USA). Detailed sample size (n) and number of replicates are shown in the figure legends. All raw data were compared by *t* tests (two groups) and one-way analysis of variance (ANOVA) with Bonferroni comparison tests (multiple groups). A value of $P < 0.05$ was considered statistically significant.

Reporting summary

Further information on research design is available in the Nature Portfolio Reporting Summary linked to this article.

Data availability

All data supporting the findings of this study are available upon reasonable request to the corresponding author. All uncropped and unedited blot images are included as Supplementary Figs. 11–36. The source data behind the graphs in the main manuscript can be found in Supplementary Data 1.

Received: 7 August 2024; Accepted: 20 May 2025;
Published online: 30 May 2025

References

1. Roda, G. et al. Crohn's disease. *Nat. Rev. Dis. Prim.* **6**, 22 (2020).
2. Torres, J., Mehandru, S., Colombel, J.-F. & Peyrin-Biroulet, L. Crohn's disease. *Lancet Lond. Engl.* **389**, 1741–1755 (2017).
3. G. B. D. 2017 Inflammatory Bowel Disease Collaborators The global, regional, and national burden of inflammatory bowel disease in 195 countries and territories, 1990-2017: a systematic analysis for the Global Burden of Disease Study 2017. *Lancet Gastroenterol. Hepatol.* **5**, 17–30 (2020).
4. Li, N. & Shi, R.-H. Updated review on immune factors in pathogenesis of Crohn's disease. *World J. Gastroenterol.* **24**, 15–22 (2018).
5. Bertani, L. Treatment and management of chronic inflammatory bowel diseases: optimizing present and future therapeutic choices. *J. Clin. Med.* **11**, 5267 (2022).

6. Núñez, F. P., Quera, R., Bay, C., Castro, F. & Mezzano, G. Drug-induced liver injury used in the treatment of inflammatory bowel disease. *J. Crohns Colitis* **16**, 1168–1176 (2022).
7. Jeong, D.Y. Induction and maintenance treatment of inflammatory bowel disease: a comprehensive review. *Autoimmun. Rev.* **18**, 439–454 (2019).
8. Li, S.-N. & Wu, J.-F. TGF-β/SMAD signaling regulation of mesenchymal stem cells in adipocyte commitment. *Stem Cell Res. Ther.* **11**, 41 (2020).
9. Brose, T. Z., Kubosch, E. J., Schmal, H., Stoddart, M. J. & Armiento, A. R. Crosstalk between mesenchymal stromal cells and chondrocytes: the hidden therapeutic potential for cartilage regeneration. *Stem Cell Rev. Rep.* **17**, 1647–1665 (2021).
10. Abou Nader, Z., Espéli, M., Balabanian, K. & Lemos, P. J. Culture, expansion and differentiation of mouse bone-derived mesenchymal stromal cells. *Methods Mol. Biol. Clifton NJ* **2308**, 35–46 (2021).
11. Yao, Z. et al. CCL2 is a critical mechano-responsive mediator in crosstalk between osteoblasts and bone mesenchymal stromal cells. *FASEB J. Publ. Fed. Am. Soc. Exp. Biol.* **35**, e21851 (2021).
12. Feng, X. et al. Mesenchymal stem cells alleviate mouse liver fibrosis by inhibiting pathogenic function of intrahepatic B cells. *Hepatol. Baltim.* 81, 1221–1227 (2024).
13. Chen, W. et al. MSC-derived exosomes attenuate hepatic fibrosis in primary sclerosing cholangitis through inhibition of Th17 differentiation. *Asian J. Pharm. Sci.* **19**, 100889 (2024).
14. Zhou, J. et al. Mesenchymal stem cell treatment restores liver macrophages homeostasis to alleviate mouse acute liver injury revealed by single-cell analysis. *Pharmacol. Res.* **179**, 106229 (2022).
15. Yang, H., Cheong, S., He, Y. & Lu, F. Mesenchymal stem cell-based therapy for autoimmune-related fibrotic skin diseases-systemic sclerosis and sclerodermatous graft-versus-host disease. *Stem Cell Res. Ther.* **14**, 372 (2023).
16. Wang, R. et al. Stem cell therapy for Crohn's disease: systematic review and meta-analysis of preclinical and clinical studies. *Stem Cell Res. Ther.* **12**, 463 (2021).
17. Vieujean, S. et al. Mesenchymal stem cell injection in Crohn's disease strictures: a phase I-II clinical study. *J. Crohns Colitis* **16**, 506–510 (2022).
18. Wade, H. et al. Akkermansia muciniphila and its membrane protein ameliorates intestinal inflammatory stress and promotes epithelial wound healing via CREBH and miR-143/145. *J. Biomed. Sci.* **30**, 38 (2023).
19. Firth, S. M. & Baxter, R. C. Cellular actions of the insulin-like growth factor binding proteins. *Endocr. Rev.* **23**, 824–854 (2002).
20. Katoh, M. et al. Vaccine therapy for heart failure targeting the inflammatory cytokine Igfbp7. *Circulation* **150**, 374–389 (2024).
21. Fu, P., Yang, Z. & Bach, L. A. Prohibitin-2 binding modulates insulin-like growth factor-binding protein-6 (IGFBP-6)-induced rhabdomyosarcoma cell migration. *J. Biol. Chem.* **288**, 29890–29900 (2013).
22. Damon, S. E., Maddison, L., Ware, J. L. & Plymate, S. R. Overexpression of an inhibitory insulin-like growth factor binding protein (IGFBP), IGFBP-4, delays onset of prostate tumor formation. *Endocrinology* **139**, 3456–3464 (1998).
23. Daza, D. O., Sundström, G., Bergqvist, C. A., Duan, C. & Larhammar, D. Evolution of the insulin-like growth factor binding protein (IGFBP) family. *Endocrinology* **152**, 2278–2289 (2011).
24. DeMambro, V. E. et al. Gender-specific changes in bone turnover and skeletal architecture in IGFBP-2-null mice. *Endocrinology* **149**, 2051–2061 (2008).
25. Xue, Y. et al. Insulin-like growth factor binding protein 4 enhances cardiomyocytes induction in murine-induced pluripotent stem cells. *J. Cell. Biochem.* **115**, 1495–1504 (2014).
26. Yan, X., Baxter, R. C., Perbal, B. & Firth, S. M. The aminoterminal insulin-like growth factor (IGF) binding domain of IGF binding protein-3 cannot be functionally substituted by the structurally homologous domain of CCN3. *Endocrinology* **147**, 5268–5274 (2006).
27. Chen, B. et al. AMPK: a bridge between inflammation and metabolism. *JSM Atherosclerosis* **1**, 1008–1016 (2016).
28. Yang, J. et al. Activation of sirt1/FXR signaling pathway attenuates triptolide-induced hepatotoxicity in rats. *Front. Pharm.* **9**, 260 (2017).
29. Li, T. et al. Picroside II alleviates liver injury induced by alpha-naphthylisothiocyanate through AMPK-FXR pathway. *Toxicol. Appl. Pharmacol.* **408**, 115248 (2020).
30. Renga, B. et al. FXR mediates a chromatin looping in the GR promoter thus promoting the resolution of colitis in rodents. *Pharmacol. Res.* **77**, 1–10 (2013).
31. Vavassori, P., Mencarelli, A., Renga, B., Distrutti, E. & Fiorucci, S. The bile acid receptor FXR is a modulator of intestinal innate immunity. *J. Immunol. Baltim.***183**, 6251–6261 (2009).
32. Strober, W., Nakamura, K. & Kitani, A. The SAMP1/Yit mouse: another step closer to modeling human inflammatory bowel disease. *J. Clin. Invest.* **107**, 667–670 (2001).
33. Xiang, S. et al. Standards of clinical-grade mesenchymal stromal cell preparation and quality control (2020 China Version). *J. Neurorestoratol.***8**, 197–216 (2020).
34. Glennie, S. et al. Bone marrow mesenchymal stem cells induce division arrest anergy of activated T cells. *Blood* **105**, 2821–2827 (2005).
35. Majumdar, M. K. et al. Characterization and functionality of cell surface molecules on human mesenchymal stem cells. *J. Biomed. Sci.* **10**, 228–241 (2003).
36. Ren, G. et al. Mesenchymal stem cell-mediated immunosuppression occurs via concerted action of chemokines and nitric oxide. *Cell Stem Cell* **2**, 141–150 (2008).
37. Ren, G. et al. Inflammatory cytokine-induced intercellular adhesion molecule-1 and vascular cell adhesion molecule-1 in mesenchymal stem cells are critical for immunosuppression. *J. Immunol.* **184**, 2321–2328 (2010).
38. Gieseke, F. et al. Proinflammatory stimuli induce galectin-9 in human mesenchymal stromal cells to suppress T-cell proliferation. *Eur. J. Immunol.* **43**, 2741–2749 (2013).
39. Luz-Crawford, P. et al. Mesenchymal stem cell-derived interleukin 1 receptor antagonist promotes macrophage polarization and inhibits B cell differentiation. *Stem Cells* **34**, 483–492 (2016).
40. Rafei, M. et al. Mesenchymal stromal cell–derived CCL2 suppresses plasma cell immunoglobulin production via STAT3 inactivation and PAX5 induction. *Blood* **112**, 4991–4998 (2008).
41. Saldanha-Araujo, F. et al. Mesenchymal stem cells promote the sustained expression of CD69 on activated T lymphocytes: roles of canonical and non-canonical NF-κB signalling. *J. Cell Mol. Med.* **16**, 1232–1244 (2012).
42. Li, A. et al. Mesenchymal stem cell therapy: hope for patients with systemic lupus erythematosus. *Front. Immunol.* **12**, 728190 (2021).
43. Doran, A. C. et al. Efferocytosis in health and disease. *Nat. Rev. Immunol.* **20**, 254–267 (2020).
44. Wang, S. et al. Targeted therapy for inflammatory diseases with mesenchymal stem cells and their derived exosomes: from basic to clinics. *Int. J. Nanomed.* **17**, 1757–1781 (2022).
45. Usunier, B. et al. HGF and TSG-6 released by mesenchymal stem cells attenuate colon radiation-induced fibrosis. *Int. J. Mol. Sci.* **22**, 1790 (2021).
46. Wang, Y. et al. Intestinal fibrosis in inflammatory bowel disease and the prospects of mesenchymal stem cell therapy. *Front. Immunol.* **13**, 835005 (2022).
47. Gu, L. et al. Exosomal microRNA-181a derived from mesenchymal stem cells improves gut microbiota composition, barrier function, and inflammatory status in an experimental colitis model. *Front. Med.* **8**, 660614 (2021).

48. Hammond, S. M. An overview of microRNAs. *Adv. Drug Deliv. Rev.* **87**, 3–14 (2015).
49. Boada-Romero, E. et al. The clearance of dead cells by efferocytosis. *Nat. Rev. Mol. Cell Biol.* **21**, 398–414 (2020).
50. Morioka, S. et al. Living on the edge: efferocytosis at the interface of homeostasis and pathology. *Immunity* **50**, 1149–1162 (2019).
51. Perry, J. S. A. et al. Interpreting an apoptotic corpse as anti-inflammatory involves a chloride sensing pathway. *Nat. Cell Biol.* **21**, 1532–1543 (2019).
52. Zhang, S. et al. Efferocytosis fuels requirements of fatty acid oxidation and the electron transport chain to polarize macrophages for tissue repair. *Cell Metab.* **29**, 443–456.e5 (2019).
53. Friedenstein, A. J. et al. Fibroblast precursors in normal and irradiated mouse hematopoietic organs. *Exp. Hematol.* **4**, 267–274 (1976).
54. Kuhbier, J. W. et al. Isolation, characterization, differentiation, and application of adipose-derived stem cells. *Adv. Biochem Eng. Biotechnol.* **123**, 55–105 (2010).
55. Erices, A. et al. Mesenchymal progenitor cells in human umbilical cord blood. *Br. J. Haematol.* **109**, 235–242 (2000).
56. Sabapathy, V. et al. Long-Term cultured human term placenta-derived mesenchymal stem cells of maternal origin displays plasticity. *Stem Cells Int* **2012**, 174328 (2012).
57. Gronthos, S. et al. Postnatal human dental pulp stem cells (DPSCs) in vitro and in vivo. *Proc. Natl. Acad. Sci. USA* **97**, 13625–13630 (2000).
58. Pethe, P. & Kale, V. Placenta: a gold mine for translational research and regenerative medicine. *Reprod. Biol.* **21**, 100508 (2021).
59. Barlow, S. et al. Comparison of human placenta- and bone marrow-derived multipotent mesenchymal stem cells. *Stem Cells Dev.* **17**, 1095–1107 (2008).
60. Silini, A. R. et al. Perinatal derivatives: where do we stand? A roadmap of the human placenta and consensus for tissue and cell nomenclature. *Front. Bioeng. Biotechnol.* **17**, 610544 (2020).
61. Dhere, T. et al. The safety of autologous and metabolically fit bone marrow mesenchymal stromal cells in medically refractory Crohn's disease - a phase 1 trial with three doses. *Aliment. Pharmacol. Ther.* **44**, 471–481 (2016).
62. Duijvestein, M. et al. Autologous bone marrow-derived mesenchymal stromal cell treatment for refractory luminal Crohn's disease: results of a phase I study. *Gut* **59**, 1662–1669 (2010).
63. Snowden, J. A. et al. Autologous stem cell transplantation in severe treatment-resistant Crohn's disease: long-term follow-up of UK patients treated on compassionate basis. *QJM Mon. J. Assoc. Physicians* **107**, 871–877 (2014).
64. Gregoire, C. et al. Allogeneic mesenchymal stromal cells for refractory luminal Crohn's disease: A phase I-II study. *Dig. Liver Dis. J. Ital. Soc. Gastroenterol. Ital. Assoc. Study Liver* **50**, 1251–1255 (2018).
65. Mizoguchi, E. et al. Recent updates on the basic mechanisms and pathogenesis of inflammatory bowel diseases in experimental animal models. *Intest. Res.* **18**, 151–167 (2020).
66. Matsumoto, S. et al. Inflammatory bowel disease-like enteritis and caecitis in a senescence accelerated mouse P1/Yit strain. *Gut* **43**, 71–78 (1998).
67. Hoffmann, J. C., Pawlowski, N. N., Kühl, A. A., Höhne, W. & Zeitz, M. Animal models of inflammatory bowel disease: an overview. *Pathobiol. J. Immunopathol. Mol. Cell. Biol.* **70**, 121–130 (2002).
68. Kosiewicz, M. M. et al. Th1-type responses mediate spontaneous ileitis in a novel murine model of Crohn's disease. *J. Clin. Invest.* **107**, 695–702 (2001).
69. Zhao, L., Chen, S., Shi, X., Cao, H. & Li, L. A pooled analysis of mesenchymal stem cell-based therapy for liver disease. *Stem Cell Res. Ther.* **9**, 72 (2018).
70. Suk, K. T. et al. Transplantation with autologous bone marrow-derived mesenchymal stem cells for alcoholic cirrhosis: phase 2 trial. *Hepatol. Baltim.***64**, 2185–2197 (2016).
71. Ticho, A. L., Malhotra, P., Dudeja, P. K., Gill, R. K. & Alrefai, W. A. Bile acid receptors and gastrointestinal functions. *Liver Res*. **3**, 31–39 (2019).
72. Gadaleta, R. M. et al. Farnesoid X receptor activation inhibits inflammation and preserves the intestinal barrier in inflammatory bowel disease. *Gut* **60**, 463–472 (2011).
73. Fiorucci, S. et al. Bile acid signaling in inflammatory bowel diseases. *Dig. Dis. Sci.* **66**, 674–693 (2021).
74. Maridas, D. E., DeMambro, V. E., Le, P. T., Mohan, S. & Rosen, C. J. IGFBP4 is required for adipogenesis and influences the distribution of adipose depots. *Endocrinology* **158**, 3488–3500 (2017).
75. Maridas, D. E. et al. IGFBP-4 regulates adult skeletal growth in a sex-specific manner. *J. Endocrinol.* **233**, 131–144 (2017).
76. Yang, B. et al. Overexpression of lncRNA IGFBP4-1 reprograms energy metabolism to promote lung cancer progression. *Mol. Cancer* **16**, 154 (2017).
77. Xi, Y., Liu, J. & Shen, G. Low expression of IGFBP4 and TAGLN accelerate the poor overall survival of osteosarcoma. *Sci. Rep.* **12**, 9298 (2022).
78. Tao, L. et al. Activation of IGFBP4 via unconventional mechanism of miRNA attenuates metastasis of intrahepatic cholangiocarcinoma. *Hepatol. Int.* **18**, 91–107 (2024).
79. Lee, Y.-Y. et al. Loss of tumor suppressor IGFBP4 drives epigenetic reprogramming in hepatic carcinogenesis. *Nucleic Acids Res*. **46**, 8832–8847 (2018).
80. Cao, H. et al. Therapeutic potential of transplanted placental mesenchymal stem cells in treating Chinese miniature pigs with acute liver failure. *BMC Med*. **10**, 56 (2012).
81. Dominici, M. et al. Minimal criteria for defining multipotent mesenchymal stromal cells. The international society for cellular therapy position statement. *Cytotherapy* **8**, 315–317 (2006).
82. Sato, T. et al. Single Lgr5 stem cells build crypt-villus structures in vitro without a mesenchymal niche. *Nature* **459**, 262–265 (2009).
83. Sato, T. et al. Long-term expansion of epithelial organoids from human colon, adenoma, adenocarcinoma, and Barrett's epithelium. *Gastroenterology* **141**, 1762–1772 (2011).
84. Yang, H. et al. Human induced pluripotent stem cell-derived mesenchymal stem cells promote healing via TNF-α-stimulated gene-6 in inflammatory bowel disease models. *Cell Death Dis.* **10**, 718 (2019).
85. Alex, P. et al. Distinct cytokine patterns identified from multiplex profiles of murine DSS and TNBS-induced colitis. *Inflamm. Bowel Dis.* **15**, 341–352 (2009).
86. Singh, P. et al. Effect of polyunsaturated fatty acids on postnatal ileum development using the fat-1 transgenic mouse model. *Pediatr. Res.* **85**, 556–565 (2019).

Acknowledgements

This work was supported by Stem Cell and Translational Research from National Key Research and Development Program of China (No. 2020YFA0113003), Central Guidance Fund for Local Science and Technology Development (No. 2024ZY01054), Fundamental Research Funds for the Central Universities (No. 2025ZFJH03), and High-level Personnel Cultivating Project of Zhejiang Province (No. 2023R5243). We thank C.B. and X.H. from the Core Facilities, Zhejiang University School of Medicine for their technical support.

Author contributions

R.W., H.C., and J.X. contributed to the research conception and design. R.W., B.F., Q.Y., and Q.P. performed the experiments. J.Y., C.L., and J.W. performed data analysis. R.W., B.F., and H.C. drafted the manuscript. L.L. supervised the study. All the authors reviewed and approved the final version of the manuscript.

Competing interests

The authors declare no competing interests.

Ethics approval

The study was approved by the Animal Experimental Ethical Inspection of The First Affiliated Hospital of Zhejiang University School of Medicine (Reference number: 2020-1088) and the Clinical Research Ethics Committee of The First Affiliated Hospital of Zhejiang University School of Medicine (Reference number: 2021-158).

Additional information

Supplementary information The online version contains supplementary material available at https://doi.org/10.1038/s42003-025-08261-y.

Correspondence and requests for materials should be addressed to Hongcui Cao or Jue Xie.

Peer review information *Communications Biology* thanks the anonymous reviewers for their contribution to the peer review of this work. Primary Handling Editor: Dr K.R.